

Effect of particle-fiber friction coefficient on ultrafine aerosol particles clogging in nanofiber based filter

Wannes Sambaer, Martin Zatloukal, and Dusan Kimmer

Citation: *AIP Conf. Proc.* **1526**, 326 (2013); doi: 10.1063/1.4802627

View online: <http://dx.doi.org/10.1063/1.4802627>

View Table of Contents: <http://proceedings.aip.org/dbt/dbt.jsp?KEY=APCPCS&Volume=1526&Issue=1>

Published by the *AIP Publishing LLC*.

Additional information on AIP Conf. Proc.

Journal Homepage: <http://proceedings.aip.org/>

Journal Information: http://proceedings.aip.org/about/about_the_proceedings

Top downloads: http://proceedings.aip.org/dbt/most_downloaded.jsp?KEY=APCPCS

Information for Authors: http://proceedings.aip.org/authors/information_for_authors

ADVERTISEMENT



AIPAdvances

Submit Now

**Explore AIP's new
open-access journal**

- **Article-level metrics
now available**
- **Join the conversation!
Rate & comment on articles**

Effect of Particle-Fiber Friction Coefficient on Ultrafine Aerosol Particles Clogging in Nanofiber Based Filter

Wannes Sambaer^{a,b}, Martin Zatloukal^{a,b} and Dusan Kimmer^c

^a*Polymer Centre, Faculty of Technology, Tomas Bata University in Zlin, TGM 275, 762 72 Zlin, Czech Republic*

^b*Centre of Polymer Systems, University Institute, Tomas Bata University in Zlin, Nad Ovcirnou 3685, 760 01 Zlin, Czech Republic*

^c*SPUR a.s., trida Tomase Bati 299, Louky, 763 02 Zlin, Czech Republic*

Abstract. Realistic SEM image based 3D filter model considering transition/free molecular flow regime, Brownian diffusion, aerodynamic slip, particle-fiber and particle-particle interactions together with a novel Euclidian distance map based methodology for the pressure drop calculation has been utilized for a polyurethane nanofiber based filter prepared via electrospinning process in order to more deeply understand the effect of particle-fiber friction coefficient on filter clogging and basic filter characteristics. Based on the performed theoretical analysis, it has been revealed that the increase in the fiber-particle friction coefficient causes, firstly, more weaker particle penetration in the filter, creation of dense top layers and generation of higher pressure drop (surface filtration) in comparison with lower particle-fiber friction coefficient filter for which deeper particle penetration takes place (depth filtration), secondly, higher filtration efficiency, thirdly, higher quality factor and finally, higher quality factor sensitivity to the increased collected particle mass. Moreover, it has been revealed that even if the particle-fiber friction coefficient is different, the cake morphology is very similar.

Keywords: Nanofibers, Electrospinning, 3D Modeling, Clogging.

PACS: 81.07.-b

INTRODUCTION

Fibrous based air filters are widely used in many applications in area of pharmaceutical, medical, biology, food, semi-conductor industries and therefore it is not surprising that both experimental [1-3] and theoretical studies [4-11] dealing with their basic characteristics (such as the pressure drop and particle collection efficiency) can be found in the open literature. It has been shown theoretically and experimentally that the particles accumulation in the filter happened in the following three stages. Firstly, particles are touched to the surface of the filter media (capillary deposition), i.e. there are particle-fiber interactions only. In the second stage, capillary deposition together with interception of already caught particles (capillary clogging) takes place, i.e. there are both, particle-fiber as well as particle-particle interactions. In the final stage, the particles are caught by the interception of other particles only, which leads to a large increase in cake growth, i.e. there are particle-particle interactions only.

Novel Trends in Rheology V

AIP Conf. Proc. 1526, 326-337 (2013); doi: 10.1063/1.4802627
© 2013 AIP Publishing LLC 978-0-7354-1151-7/\$30.00

A number of theoretical studies considering the above described filter clogging mechanism [12-22] have already been performed for micro-fibrous filters.

Nowadays, nanofiber nonwoven based filters becomes of high interest due to their ability to reach high filtration efficiency for ultrafine particles with a low pressure drop due to aerodynamic slip around the nanofibers. Unfortunately, till now, the detailed theoretical analysis of the nanofiber based filters clogging has not been performed yet and thus, the full understanding of the filtration cake formation on the nanofiber based filters and its role on the final filter efficiency is not fully understood yet. In order to provide a better understanding of the nanofiber based filters loading process with respect to pressure drop and filtration efficiency evolution, UTBsoft Filtration v1.0.0 simulation software recently developed by authors from Tomas Bata University in Zlín (utilizing a realistic SEM image based 3D structure model of the filter, transition/free molecular flow regime, Brownian diffusion, particle-fiber interactions, aerodynamic slip and sieve) has been utilized in this work.

FILTER PREPARATION AND CHARACTERIZATION

Materials

A polyurethane solution in dimethylformamide (DMF) based on 4,4'-methylenebis(phenylisocyanate) (MDI), poly(3-methyl-1,5-pentanediol)-alt-(adipic, isophthalic acid) (PAIM) and 1,4 butanediol (BD) was synthesized in molar ratio 9:1:8 at 90°C for 5 hours (per partes way of synthesis starting with preparation of prepolymer from MDI and PAIM and followed by addition of BD and remaining quantity of MDI). The prepared solution was suitable for electrospinning process and had a PU concentration of 24.1 wt.%, viscosity of 1.45 Pa.s and conductivity of 157 μ S.cm⁻¹ (adjusted by 3 parts of citric acid and 1 part of borax).

Electrospinning Process

In this work, a commercially available NanoSpiderTM machine (Elmarco s.r.o. Liberec, Czech Republic, <http://www.elmarco.com/>) equipped with patented (PCT/CZ2010/000042) rotating electrode with 3 cotton cords spinning elements was used to prepare nanofiber nonwoven based filter sample from polyurethane solution. The experimental conditions were: relative humidity 25 %, temperature 23.5°C, high voltage applied into PU solution 75 kV, distance between electrodes 210 mm, rotational electrode speed 7 rpm and speed of polyester nonwoven supporting textile collecting nanofibers was 0.4 m.min⁻¹. Samples for further analyses were taken from the middle part of the 40 cm wide fabric coated with layer of nanofibers.

Nanofiber Filter Characterization

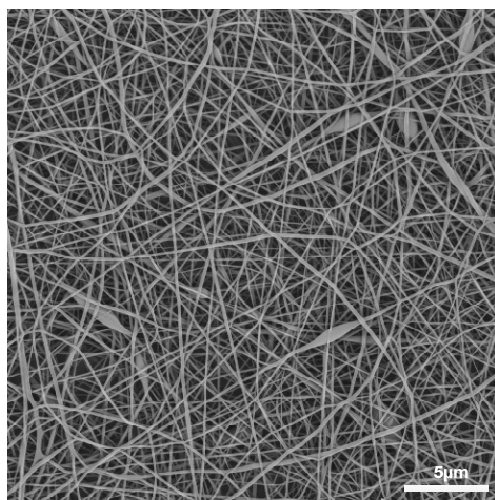


FIGURE 1. SEM image of the manufactured nanofiber based nonwoven filter.

A nanofiber based filter, prepared via electrospinning process, has been characterized by Scanning Electron Microscope technique (Vega 3, Tescan, Czech republic), as visible in Figure 1. The obtained SEM picture has consequently been used for the fiber diameter/pore size distribution determination by using recently proposed digital image analysis technique [24]. The filter has an average fiber diameter and average pore size equal to 133 nm and 156 nm, respectively, thickness of 3.59 μm and mass area of 0.54 g.m⁻². The electric potential generated on the surface of the filter was measured by electrostatic fieldmeter Simco, model FMX-003, the Netherlands. It has been found that the surface charge potential of the filter was practically negligible, equal to 70 V, i.e. there are practically no electrostatic forces, which could affect its filtration characteristics. The filtration efficiency for the prepared nanofiber based filter was determined experimentally in the ultrafine particle range according to following procedure. An ammonium sulphate solution having concentration of 1 g.l⁻¹ was nebulized (AGK, PALAS, Germany), a monodisperse size fraction was selected using an Electrostatic Classifier (EC 3080, TSI, USA) and particle concentration upstream and downstream the filter (face velocity 5.7 cm/s) was recorded by a condensation particle counter (UCPC 3025 A, TSI, USA). The filtration efficiency was determined at nine mobility diameter fractions (20, 35, 50, 70, 100, 140, 200, 280 and 400 nm). Note that the filtration efficiency and pressure drop measurements were repeated four times and the following filtration efficiency characteristics of the filter were experimentally determined: the Maximum Penetration Pore Size (MPPS) 70 nm, the minimum filtration efficiency 98.32%, the average pressure drop 148.5 Pa and the quality factor 27.5 kPa⁻¹, which is defined according to Eq. 1.

$$QF = -\frac{\ln E}{\Delta p} \quad (1)$$

where Δp is the pressure drop and E is the filtration efficiency at MPPS.

FILTER MODEL DESCRIPTION

3D Filter Structure Model

The 3D filter model has been generated from SEM image by using recently proposed methodology [25] in order to take varying fiber diameter, curvature and possible structure defects as well as 3D features of the whole filter correctly into account. Figure 2 shows the 3D structure model for the investigated polyurethane nanofiber based filter created from the SEM image depicted in Figure 1 according to the technique described in [25].

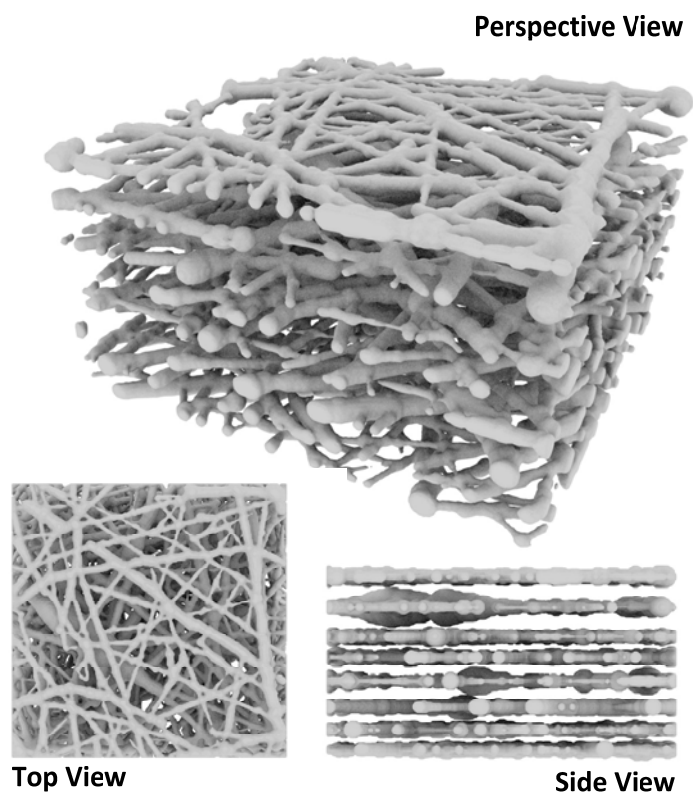


FIGURE 2. Full 3D structure model, in perspective, top and side view, of the manufactured filter.

Flow Field Calculation

The transition-free molecular flow regime is considered in this work due to small average fiber diameter size (133 nm) of the investigated filter for which the Knudsen number, calculated as the ratio of two times gas molecules mean free path and fiber diameter, is higher than 0.25. In such a case, particle Brownian motion and uniform gas flow field can only be considered as a result of significant air slip occurrence at the fiber surface where the influence of the fibers on the flow field is negligible as suggested by Maze et al. [7]. In such a case, the flow field is described by the set of equations, which are summarized in [25].

Particle-Fiber Interaction Modeling

In this work, the flow through the particular pore is viewed as the Poiseuille slip flow in a circular duct, having the gap distance, H , where the drag force F_D , the lift force F_L , the adhesion (van der Waals) force F_A , and the friction force F_F are considered to act between the fiber and a non-deformable spherical particle according to J. Altmann and S. Ripperger [26] (see Figure 3).

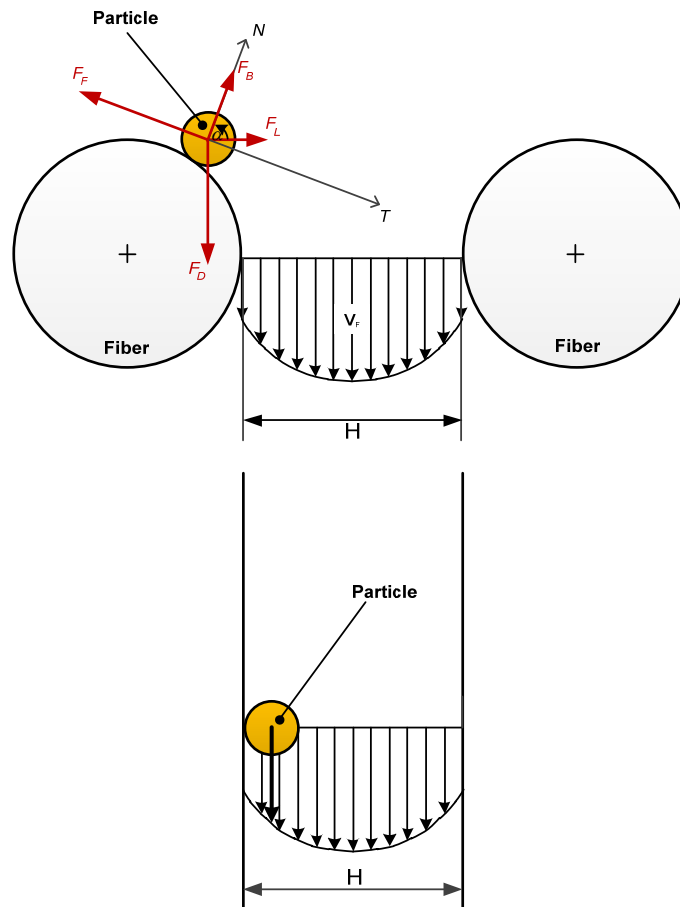


FIGURE 3. Fiber local coordinate system based force balance utilized for particle-fiber interaction modeling.

In more detail, the *drag force*, F_D , starts to act on the fiber intercepted particle due to pressure driven shear flow occurring inside the pore having average diameter H determined here as the perpendicular distance between the interception particle/fiber point and surrounding fiber, which represents the second part of the pore. The local fiber wall shear stress τ_w , which can be calculated from the Newtonian law using the gas viscosity and the shear rate at the fiber wall calculated as proposed by Barber and Emerson [27]. The equation for the *lift force*, F_L , which is induced by the shear flow perpendicularly to the drag force, is utilized here in the form suggested by Rubin [29], J. Altmann and S. Ripperger [26] and McLaughlin [30] based on their theoretical and experimental analysis. The estimation of the *adhesion force*, F_A , is complicated

because different parameters such as particle/fiber shape, particle/fiber roughness, adhesion distance, number of contact points etc. may influence the adhesive force strongly [26]. Here, neglecting the electrostatic interactions, the adhesive forces is evaluated through the van der Waals force acting between two spheres of radii R_1 and R_2 [31]. The *friction force*, F_F , is caused by the action of the normal force, F_N , acting towards the fiber surface (i.e. sum of the van der Waals force F_A , normal component of the lift force F_{L_n} and drag force F_{D_n}) where the friction coefficient, μ , is considered here to be Knudsen number dependent parameter (i.e. in the same way as the air viscosity suggested by McNenly [28]).

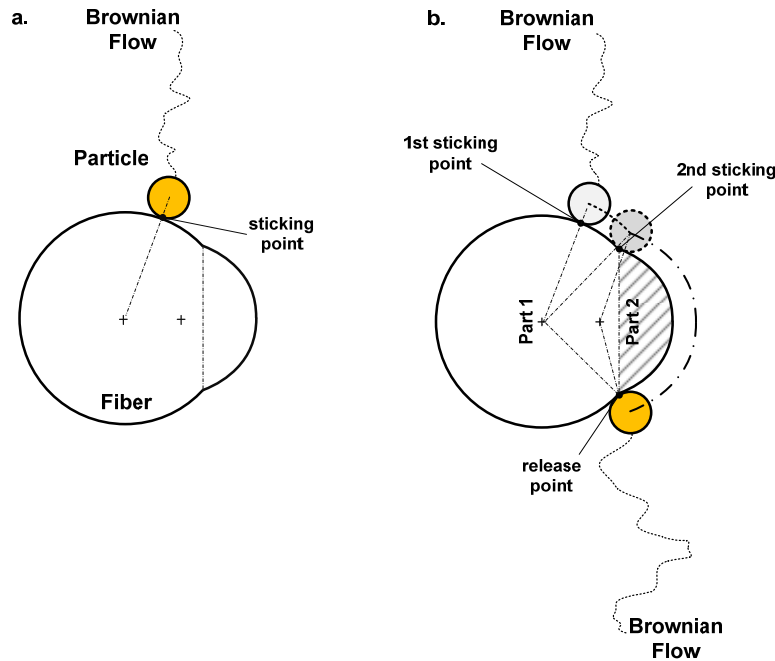


FIGURE 4. Interception (4a.) and local slip (4b.) conditions of a particle in contact with a single fiber.

The particle is considered to be intercepted (see Figure 4a.) by the fiber when the lift force is lower/equal than the adhesion force, $F_L \leq F_A$, or the drag force is lower/equal than the friction force, $F_D \leq F_F$. On the other hand, if the lift force is higher than the adhesion force ($F_L > F_A$) or the drag force is higher than the friction force ($F_D > F_F$), the particle starts to slip around the fiber in the local slip plane with respect to the particular fiber part and the particle is always released from the particular fiber part in the horizontally mirrored position with respect to initial sticking point between the particle and the particular fiber part as can be seen in Figure 4b.

It also should be mentioned that particle catching due to sieving is considered when at least two connection points between fiber1-particle-fiber2 are identified during the particle motion modeling.

Particle-Particle Interaction

In this work, the fully sticking (single touching point) boundary condition was applied for the particle-particle interaction modeling (similarly to other theoretical studies [13,15-20,32-34]) which can be justified for the 10 nm – 5 μm particle size range as showed experimentally by Wang and Kasper [35] and Pawu and Braaten [36]. Under this condition, dendrites (formed by the accumulated particles during the filtration process) cannot bend or break down in this model.

THEORETICAL PARAMETRIC STUDY AND RESULTS

The filtration efficiency of the filter is theoretically determined by the number of particles, which can be captured inside the filter [7] as shown in Eq. 2:

$$E = \frac{N_{in} - N_{out}}{N_{in}}, \quad (2)$$

where N_{in} and N_{out} are the numbers of entering and exiting particles, respectively. Twenty different groups of 10,000 identical particles having diameter linearly varying from 20 to 500 nm on a logarithmic scale were injected in the large modeled clean filter inlet having dimensions of 7.2 on 7.2 μm. In order to validated the model the efficiency, pressure drop and quality factor has been simulated and calculated on the 3D model shown in Figure 2 and it have been found that the calculated values are within the experimental error for all evaluated parameters.

For the cake formation modeling, the 3D filtration model depicted in Figure 2 was randomly penetrated with 50,000 particles, having the particle size distribution the same as the nebulized ammonium sulphate solution used in the experimental filtration test, considering both particle-fiber and particle-particle interactions. The cake formation for 0, 750, 2,500, 5,000, 7,500, 10,000, 15,000, 20,000, 25,000 and 50,000 particles on the filter tested in this work are depicted in Figure 5. Clearly, deposited particles form dendrites in the beginning of the filtration process (at the filter top and in through the depth) as well as at the end where predominant filter cake formation takes place, which is in good agreement with the open literature [12].

In order to more deeply understand the particle-fiber friction coefficient effect on the cake build up, filtration efficiency, pressure drop and quality factor of the nanofiber based filters, its value was varied from 0 to 0.025 in the utilized filtration model. The 3D filter model was randomly penetrated with 50,000 particles, with an experimentally defined particle size distribution. The filtration efficiency, the pressure drop and quality factor (calculated by Eq. 1) was recorded during the filter clogging as a function of the captured particle mass area for different particle-fiber frictions and the results are depicted in Figure 6. Clearly, the increase in the fiber-particle friction coefficient leads to higher pressure drop, higher filtration efficiency and higher quality factor. On the other hand, the filter samples with higher fiber-particle friction coefficient shows much higher quality factor reduction with the increased collected particle mass in comparison with the filter samples having lower fiber-particle friction

coefficient, as visible in Figure 6b. These trends can be understood through analysis of 3D views of all tested filters filled by the particles (see Figure 7). A decrease in the particle-fiber friction coefficient leads to deeper particle penetration in the filter, creation of less saturated top fibers (depth filtration, see Figure 8a) and generation of lower pressure drop in comparison with higher particle-fiber friction coefficient filters (surface filtration, see Figure 8b). On the other hand, the pressure drop through the filter cake was found to be comparable for all considered filters samples due to their similar morphology.

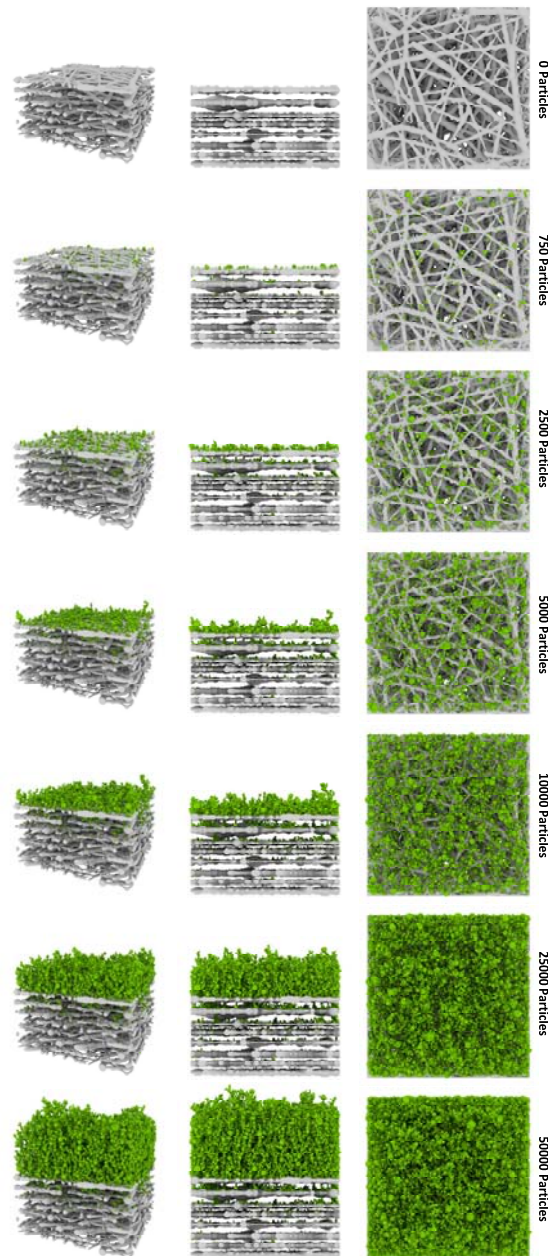


FIGURE 5. The cake filtration modeling for different number of particles (left – perspective view, middle - side view, right – top view).

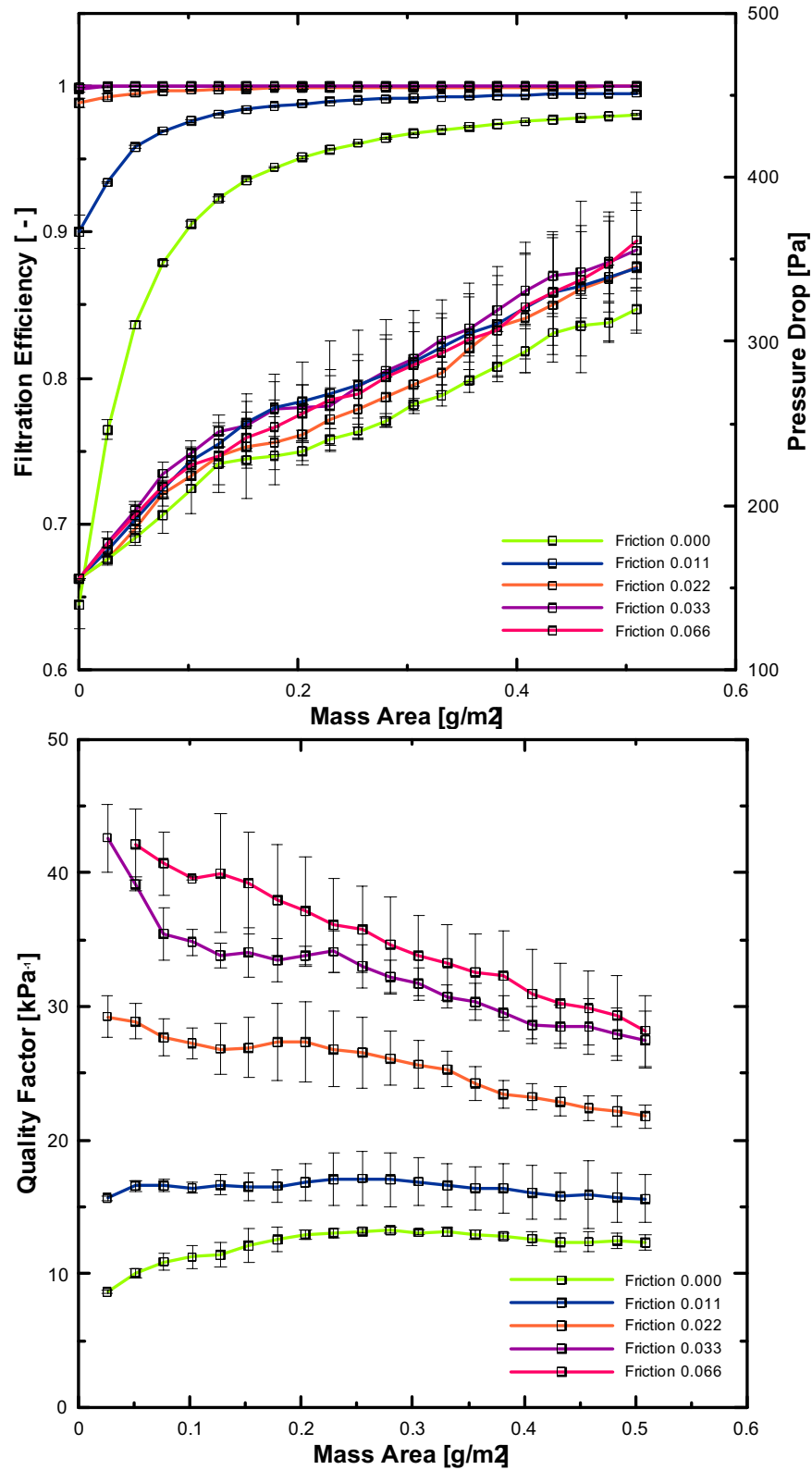


FIGURE 6. The effect of particle-fiber friction coefficient on basic filtration characteristics during particle clogging. **6a.** Filtration efficiency and pressure drop. **6b.** Quality factor.

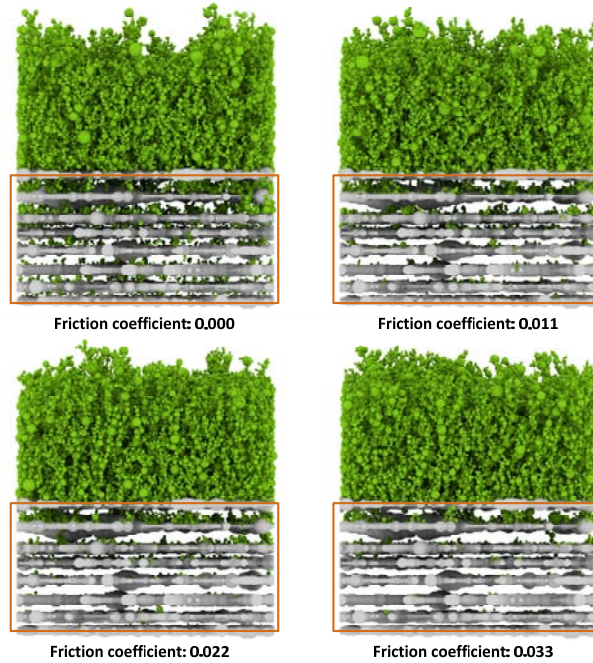


FIGURE 7. The effect of particle-fiber friction coefficient on particle penetration in the filter and cake build up for 50,000 particles.

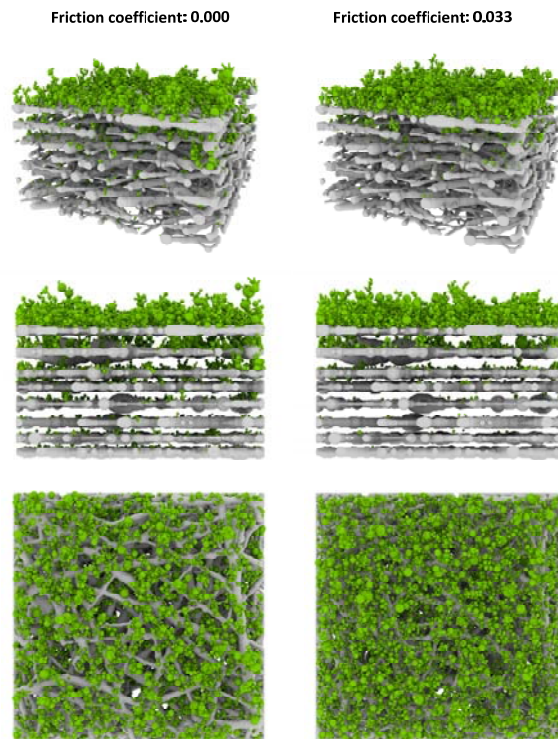


FIGURE 8. The effect of particle-fiber friction coefficient on the type of dendrite build-up in the initial stage. **8a.** low friction coefficient results in depth filtration, **8b.** high friction coefficient results in surface filtration.

CONCLUSIONS

Polyurethane nanofiber based filter has been prepared by electrospinning process having average fiber diameter and average pore size equal to 133 nm and 156 nm, respectively, thickness 3.59 μm , mass area 0.54 $\text{g}\cdot\text{m}^{-2}$, maximum penetration pore size 70 nm, minimum filtration efficiency 98.32%, average pressure drop 148.5 Pa and quality factor 27.5 kPa^{-1} .

The realistic SEM image based 3D filter model, transition/free molecular flow regime, Brownian diffusion, aerodynamic slip, particle-fiber and particle-particle interactions has been utilized for the prepared polyurethane nanofiber based filter in order to more deeply understand the filtration cake formation and its role on the final filter efficiency. The performed analysis has revealed that the cake structure formed on the analyzed nanofiber based filter is dendrites based and rather porous.

Based on the performed theoretical analysis, it has been revealed that the increase in the fiber-particle friction coefficient causes, firstly, more weaker particle penetration in the filter, creation of dense top layers and generation of higher pressure drop (surface filtration) in comparison with lower particle-fiber friction coefficient filter for which deeper particle penetration takes place (depth filtration), secondly, higher filtration efficiency, thirdly, higher quality factor and finally, higher quality factor sensitivity to the increased collected particle mass. Moreover, it has been revealed that even if the particle-fiber friction coefficient is different, the cake morphology is very similar.

ACKNOWLEDGMENTS

The authors wish to acknowledge the Grant Agency of the Czech Republic (grant No. P108/10/1325) for the financial support. This article was written with support of Operational Program Research and Development for Innovations co-funded by the European Regional Development Fund (ERDF) and national budget of Czech Republic, within the framework of project Centre of Polymer Systems (reg. number: CZ.1.05/2.1.00/03.0111).

REFERENCES

1. W. W. F. Leung, C. H. Hung and P. T. Yuen, *Aerosol Sci. Tech.* **43**, 1174-1183 (2009).
2. W. W. F. Leung, C. H. Hung and P. T. Yuen, *Sep. Purif. Technol.* **71**, 30-37 (2010).
3. A. Podgorski, A. Balazy and L. Gradon, *Chem. Eng. Sci.* **61**, 6804-6815 (2006).
4. S. A. Hosseini and H. V. Tafreshi, *Sep. Purif. Technol.* **74**, 160-169 (2010).
5. B. Zhou, P. Tronville and R. Rivers, *Fibers Polym.* **10**, 526-538 (2009).
6. W. Sambaer, M. Zatloukal and D. Kimmer, *Chem. Eng. Sci.* **66**, 613-623 (2011).
7. B. Maze, H. V. Tafreshi, Q. Wang and B. Pourdeyhimi, *J. Aerosol Sci.* **38**, 550-571 (2007).
8. S. A. Hosseini and H. V. Tafreshi, *Chem. Eng. Sci.* **65**, 2249-2254 (2010).
9. S. A. Hosseini and H. V. Tafreshi, *Power Technol.* **201**, 153-160 (2010).
10. M. Rebal, F. Drolet, D. Vidal, I. Vakeiko and F. A. Bertrand, *Asia-Pac. J. Chem. Eng.* **6**, 26-37 (2011).
11. S. Jaganathan, H. V. Tafreshi and B. Pourdeyhimi, *Chem. Eng. Sci.* **63**, 244-252 (2008).

12. T. D. Elmoe, A. Tricoli, J. Grunwaldt and S. Pratsinis, *J. Aerosol Sci.* **40**, 965-981 (2009).
13. D. Thomas, P. Penicot, P. Contal, D. Leclerc and J. Vendel, *Chem. Eng. Sci.* **56**, 3549-3561 (2001).
14. C. E. Billings, "Effects of Particle Accumulation in Aerosol Filtration", Ph.D. Thesis, California Institute of Technology, 1966.
15. C. Kanaoka, and S. Hiragi, *J. Aerosol Sci.* **21**, 127-137 (1990).
16. T. Witten and L. Sander, *Phys. Rev. Lett.* **27**, 5686-5697 (1983).
17. A. C. Payatakes and L. Gradon, *American Int. Chem. Eng. J.* **26**, 443-454 (1980).
18. C. S. Cheung, Y. H. Cao and Z. D. Yan, *Computation Mechanics* **35**, 449-458 (2005).
19. C. Kanaoka, S. Hiragi and T. Tanthapanichakoon, *Powder Technol.* **118**, 97-106 (2001).
20. B. Huang, R. Turton, J. Park, P. Famouri and E. J. Boyle, *Powder Technol.* **163**, 23-31 (2006).
21. A. Karadimos and R. Ocono, *Powder Technol.* **137**, 109-119 (2003).
22. Y. Chang, Y. Huang, Z. Luo and G. Zhang, *Sep. Purif. Technol.* **63**, 566-576 (2008).
23. W. Sambaer, M. Zatloukal, *Recent Advances in Fluid Mechanics, Heat & Mass Transfer and Biology - Proc. of the 9th WSEAS Int. Conf. on FLUIDS'12, 9th WSEAS Int. Conf. on HMT'12, 9th WSEAS Int. Conf. on MABE'12*, pp. 144-149 (2012).
24. W. Sambaer, M. Zatloukal and D. Kimmer, *Polym. Test.* **29**, 82-94 (2010).
25. W. Sambaer, M. Zatloukal and D. Kimmer, *Chem. Eng. Sci.* **82**, 299-311 (2012).
26. J. Altmann and S. Ripperger, *J. Membrane Sci.* **124**, 119-128 (1997).
27. R. W. Barber and D. R. Emerson, *Daresbury Laboratory Technical Report*, DL-TR-00-002 (2000).
28. M. J. Mcnenly, M. A. Gallis and I. D. Boyd, *Int. J. Numer. Meth. Fl.* **49**, 1169-1191 (2005).
29. G. Rubin, "Widerstand-und Auftriebsbeiwerte und rut enden, kugelförmigen Partikeln in Stationären wandnahen laminaren Grenzschichten", Ph.D. Thesis, TH Karlsruhe, Germany, 1977.
30. J. B. McLaughlin, *J. Fluid. Mech.* **246**, 249-265 (1993).
31. B. Bhushan, *Nanotribology and Nanomechanics: An Introduction*, Berlin: Springer 2005, p. 1148.
32. L. Madler, A. A. Lall and S. K. Friedlander, *Nanotechnology* **17**, 4783-4795 (2006).
33. D. Rodriguez-Perez, J. L. Castillo and J. C. Antoranz, *Phys. Rev. Lett.* **72**, 021403-1-021403-9 (2005).
34. R. Przekop and L. Gradon, *Aerosol Sci. Technol.* **42**, 483-493 (2008).
35. H. C. Wang and G. Kasper, *J. Aerosol Sci.* **22**, 31-41 (1991).
36. K. T. Pawu and D. A. Braaten, *Aerosol Sci. Tech.* **23**, 72-79 (1995).